ACS APPLIED MATERIALS & INTERFACES

www.acsami.org

Research Article

Functional Kevlar-Based Triboelectric Nanogenerator with Impact Energy-Harvesting Property for Power Source and Personal Safeguard

Jianyu Zhou, Sheng Wang,* Fang Yuan, Junshuo Zhang, Shuai Liu, Chunyu Zhao, Yu Wang, and Xinglong Gong*

Cite This: *ACS Appl. Mater. Interfaces* 2021, 13, 6575−6584

Read Online

ACCESS | Metrics & More | Article Recommendations | Supporting Information

ABSTRACT: A novel shock-resistant, self-generating triboelectric nanogenerator (SS-TENG) with high-speed impact energy-harvesting and safeguarding properties was developed by assembling Kevlar fiber and conductive shear-stiffening gel. The SS-TENG with energy-harvesting property generated a maximum power density of 5.3 mW/m^2 with a voltage of 13.1 V under oscillator compression and could light up light-emitting diode arrays. Owing to the energy absorption effect, the as-designed SS-TENG could dissipate impact forces from 2880 to 1460 N, showing anti-impact performance under the drop hammer impact. It also sensed the loading forces by outputting 36.4 V. Functionalized as a self-powered sensor, SS-TENG monitored various human movements and provided protection from hammer impact. Interestingly, a wearable sole array with high sensitivity and a fast response could distinguish toe in/out motions. More importantly, this functional SS-TENG presented excellent anti-impact behavior, which dissipated 94% of kinetic energy under bullet-shooting excitation. It also gathered high speed ballistic energy, which outputted a maximum power density of 3 mW/m^2. To this end, this SS-TENG with a protection effect and the ability to harvest various impact energy showed promising applications in new power sources, intelligent wearable systems, and safeguard areas.

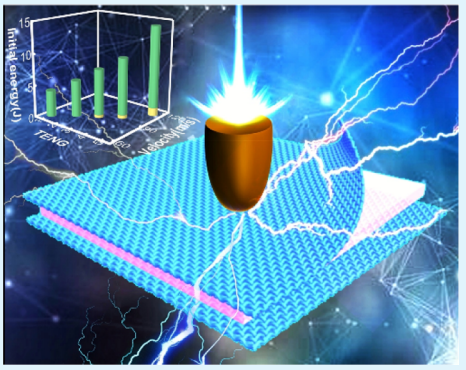

KEYWORDS: *triboelectric nanogenerator, impact energy, shear-stiffening gel, Kevlar fiber, wearable sensor*

INTRODUCTION

In recent years, energy crisis led by the exhausting fossil fuels propels scientists to develop clean and renewable power sources to meet the energy requirements of human society.[1−6] Among all the developed power devices, triboelectric nanogenerators (TENGs) show favorable application as alternative sustainable power sources in different areas.[7−11] Based on the triboelectric effect and electrostatic induction, TENG can convert various kinetic energy into electricity. Especially, with the increasing use of advanced soft electronics, wearable TENGs, owing to their advantages of high flexibility and efficiency, could be attached on the human body showing important potential for application as portable power sources.[12−15]

Textile, owing to the advantages of softness, low price, and wearing comfort, is an ideal candidate for designing wearable TENG devices. A portable TENG made of nylon and Dacron fabric could effectively harvest body motion energy and generate a voltage as high as 2 kV.[16] Smart TENGs relying on cotton socks could capture and reveal more direct sensory information on the human body including physiological motions, contact force, and sweat levels.[17] The introduction of polyacrylonitrile into TENG endowed the device with machine-washable and breathable properties.[18] Besides, as miniaturization and integration is more favorable for wearable devices, various all-in-one textile-based TENGs have been further developed by taking advantage of the superiority of fibers. Besides harvesting energy, the polyester fiber-based TENG also showed good disinfection performance toward bacteria.[19] Because of the flame-retardant yarn, a 3D honeycomb-structured TENG could work as a self-powered escape in fire rescue.[20] These results indicate functional textiles will endow TENGs with additional properties that widen their practical applications. However, currently reported TENG devices only harvest slight mechanical energy, which include human motion,[21] water dropping,[22] and wind blowing[23] energy. The triboelectric performance of most textile-TENGs easily fails under loading forces because of their weak mechanical properties.

Received: October 12, 2020
Accepted: January 21, 2021
Published: February 1, 2021

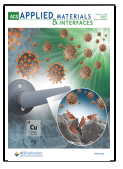

https://dx.doi.org/10.1021/acsami.0c18308
ACS Appl. Mater. Interfaces 2021, 13, 6575−6584

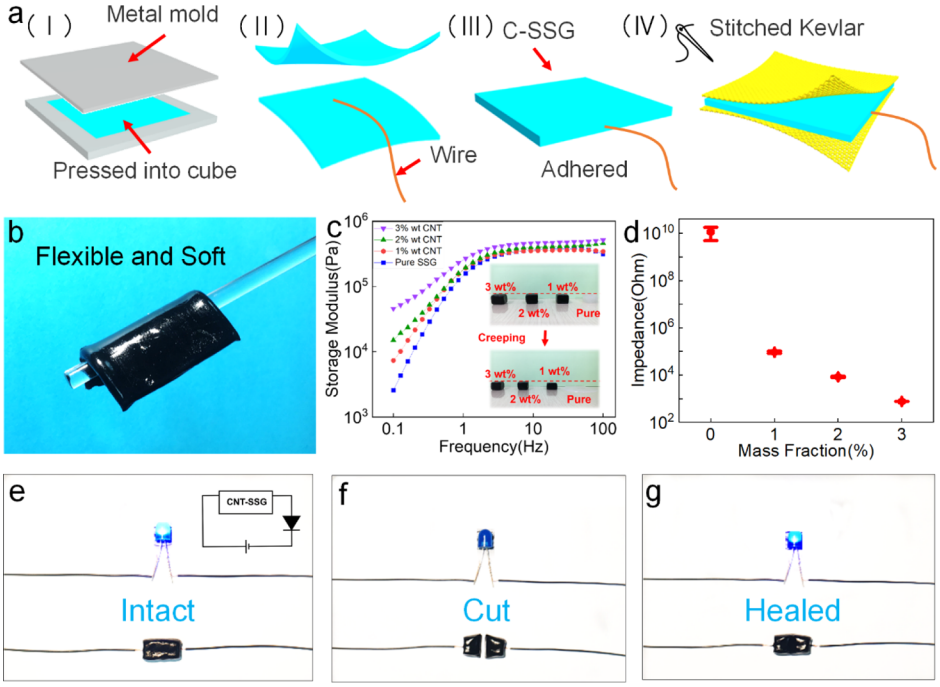

Figure 1. (a) Fabrication schematic of c-SSG/Kevlar-based SS-TENG. The c-SSG was (b) flexible and soft; (c) storage modulus of SSG with different mass ratios of CNTs under shear forces; (d) c-SSG impedance as a function of CNT contents; (e−g) digital photographs of the healing process for c-SSG.

Harmful mechanical collisions are widespread in daily life. These impacts, such as medium-speed car accidents and high-velocity bullet shooting, are always dangerous to human beings. Thus, body armor materials have become a hot research topic in recent years. Shear-thickening fluids were considered to be ideal smart materials for human body protection and they were studied in previous works.[24−26] Moreover, intelligent shear-stiffening gel (SSG), as a viscoelastic polymer, can change its modulus by four orders of magnitude.[27] The reversible soft−rigid transition property guarantees its promising application in safeguard systems. Recently, aramid Kevlar fibers with a high modulus, small fracture strain, and low density have been applied in protective areas.[28−31] Combining Kevlar with SSG has been proved to be a successful strategy for enhancing the anti-impact properties of the composites.[32] However, a previous study mainly focused on the anti-impact property of SSG/Kevlar under the impact speeds lower than 5 m/s, ignoring the mechanical performance under high-speed shooting. Besides, external power should be necessarily supplied to actuate the piezoresistive-Kevlar/SSG fiber sensor to monitor external impact forces and human movements. Because the current wearable TENGs were invalid under impact conditions, high-speed kinetic energy could not be harvested by them. They also could not detect consecutive impact excitation as self-powered sensors.[33−35] Some functional TENGs with excellent self-healing properties could recover their triboelectric as well as mechanical properties after destruction, which surely prolonged their lifespan.[36,37] However, these polymer-based TENGs still could not maintain violent impact and harvest the energy. Thus, it may be possible to develop all-in-one functional TENGs with good protection and the ability to collect various kinds of dynamic impact energies by combining SSG with Kevlar fibers.

In this work, a shock-resistant, self-generating TENG, based on Kevlar fiber and conductive shear stiffening gel (c-SSG), was developed. Under oscillator loadings of 60 N and 10 Hz, the maximum power density of SS-TENG could reach 5.3 mW/m^2 with a voltage of 13.1 V. Besides, SS-TENG effectively absorbed and dissipated drop hammer impact force by 60.8%, providing protection for humans. With the increasing of falling heights, the electrical signals also increased with the maximum value of 63.8 V. Therefore, the wearable SS-TENG as well as the based-sole array could sense and analyze various human motions. Finally, the SS-TENG device showed excellent anti-ballistic property, which resisted bullet shooting with 76.3 m/s. It also harvested the harsh impact energy by generating a power density of 3 mW/m^2 and these voltage signals could be used to assess external impact.

EXPERIMENTS AND CHARACTERIZATION

Materials. Hydroxyl silicone oil and boric acid were purchased from Sinopharm Chemical Reagent Co. Ltd, Shanghai, China. Carbon nanotubes (CNTs) with a diameter of 8−13 nm and a length of 8−10 μm were provided by Conductive Materials of Heluelida Co. Ltd, Xinxiang City, Henan province, China. The fabric used in this paper was the plain-woven aramid Kevlar fabric with an areal density of 200 g/m^2. It was also commercially available. All the chemical reagents were of analytical purity and were used as received without further purification.

Fabrication of c-SSG. First, hydroxyl silicone oil and boric acid were vigorously stirred, followed by adding different amounts of CNTs. The mixture was heated in an oven at 180 °C. Then, octanoic acid was precisely dropped into the hydroxy silicone oil during the reaction using a pipette. The dosage of octanoic acid was calculated based on the requirement of 250 μL per 100 g of hydroxy silicone oil. After homogeneously mixing, the composite was heated for another 30 min. The resulting polymer was cooled to room

https://dx.doi.org/10.1021/acsami.0c18308
ACS Appl. Mater. Interfaces 2021, 13, 6575−6584

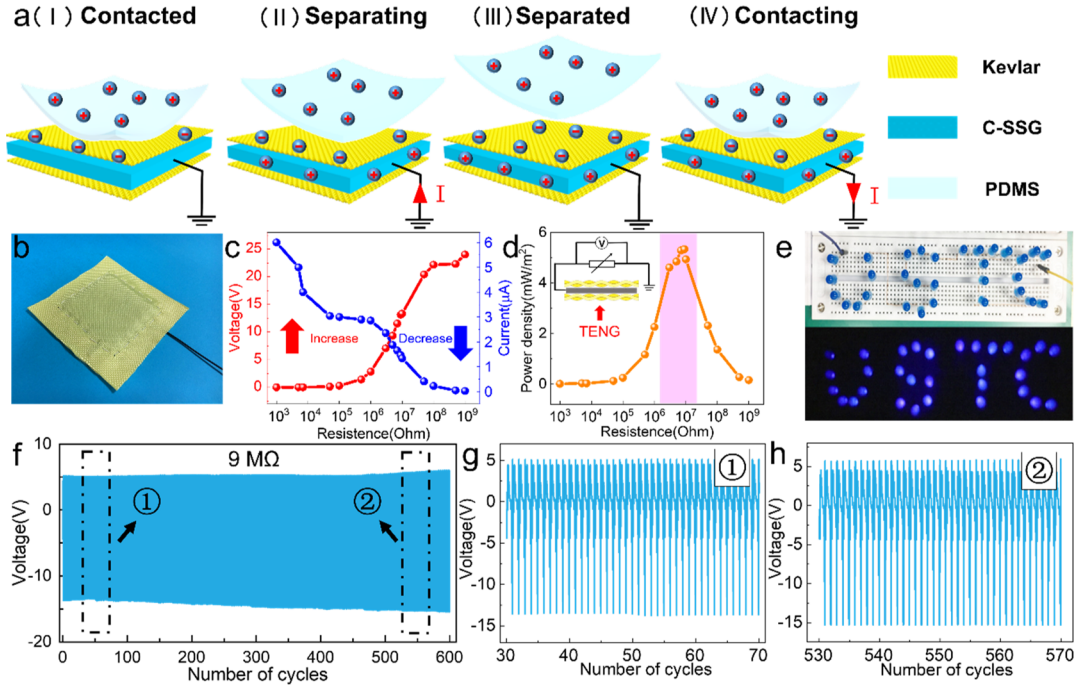

Figure 2. (a) Working mechanism of SS-TENG; (b) the as-designed c-SSG/Kevlar-based SS-TENG; (c) voltage, current, and (d) output power under various external resistance; (e) SS-TENG harvested mechanical energy and lit up LEDs; (f–h) cycling stability of SS-TENG at 9 MΩ.

temperature and blended using a two roll mill (Taihu Rubber Machinery Inc., China, Model XK-160) to obtain c-SSG.

Preparation of c-SSG/Kevlar-Based SS-TENG. c-SSG was molded into a cuboid with a cross-sectional size of 60 × 60 mm^2 and a thickness of 2 mm. A conductive wire was placed between two c-SSGs, and they were wrapped with Kevlar. The Kevlar was sewn along the edges of c-SSG. Thus, a c-SSG/Kevlar-based SS-TENG was obtained.

Characterization. The microstructures of nanoparticles and SS-TENGs were characterized by scanning electron microscopy (SEM) (Gemini SEM 500, ZEISS). Rheological properties of the polymer matrix were measured using a commercial rheometer (Physica MCR 301, Anton Paar Co., Austria). The tested samples were fixed into a cylinder with a diameter of 20 mm and a thickness of 0.85 mm. The shear frequency varied from 0.1 to 100 Hz. The triboelectric tests were conducted using an oscillator (JZK-10) (bought from Sinocera Piezotronics INC, China) and the corresponding output signals were recorded using a digital multimeter (DMM 6001). Signals are processed by using a low-pass filter. The energy-collecting and safeguarding properties of the SS-TENG device were explored using a drop hammer test system. In the high-speed bullet impact experiment, a gas gun was used to fire the bullet. A laser velocimeter was applied to measure the initial velocity of a bullet. SS-TENG was fixed to a steel frame and the wire from SS-TENG was connected with a digital oscilloscope, which was used to record voltage signals. The damage and residual speed of bullets after passing through the SS-TENG were recorded using a high-speed video camera.

RESULTS AND DISCUSSION

Characterization of c-SSG. Figure 1a shows the schematic of the preparation procedures of SS-TENG. Briefly, the CNT was introduced into SSG and mixed by a two roll mill. Then, c-SSG was molded into a rectangular shape with a volume of 60 × 60 × 2 mm^3 using a metal mold [Figure 1a(I)]. A conductive wire was fixed between two c-SSGs. Because of the viscoelasticity and chemical interaction of hydrogen bonds, the two stuck c-SSGs could clamp the wire [Figure 1a(II,III)]. The wearable SS-TENG was assembled by stitching two Kevlar fabrics with the conductive c-SSG layer [Figure 1a(IV)]. Besides, the microstructures of the composites were also studied. The SEM image of neat Kevlar fabric is shown in Figure S1a. Obviously, Kevlar bundle was smooth and there were small gaps between the fibers. Figure S1b shows the SEM image of CNTs. These carbon nanotubes with linear nanostructures entangled with each other. Pure SSG was also smooth (Figure S1c). In this work, CNTs were introduced into SSG at high temperature. Upon increasing the mass fractions from 1 to 3%, more CNTs were observed to uniformly disperse on the SSG matrix (Figure S1d–f).

c-SSG was flexible and soft, which could deform by its own weight (Figure 1b). However, this unique polymer turned to stiff under impact conditions and effectively resisted the hammer strike [Figure S2a(I,II)]. Then, it bounded several times owing to the release of storage energy [Figure S2a(III,IV)]. The height of the material slightly changed during this process. Thus, the as-designed c-SSG presented shock-resistance and energy storage properties. For the pure SSG, when the shear frequency was 0.1 Hz, the initial storage modulus (G'_{min}) was 2.6 kPa, presenting a soft viscosity state. As soon as the shear frequency reached 100 Hz, the maximum storage modulus (G'_{max}) increased to 0.3 MPa, exhibiting a typical shear-stiffening effect. Thus, pure SSG was so soft that it could hardly sustain its shape. SSG with a height of 1.5 cm collapsed into a flat shape within 48 h (inset figure in Figure 1c). Interestingly, SSG with CNTs showed high stability, which could remain stable during this period. Undoubtedly, the rheological properties of the composites were increased by introducing CNTs. For example, the G'_{max} values of c-SSG with 2 and 3% CNTs were 0.46 and 0.51 MPa, respectively. Besides,

https://dx.doi.org/10.1021/acsami.0c18308
ACS Appl. Mater. Interfaces 2021, 13, 6575–6584

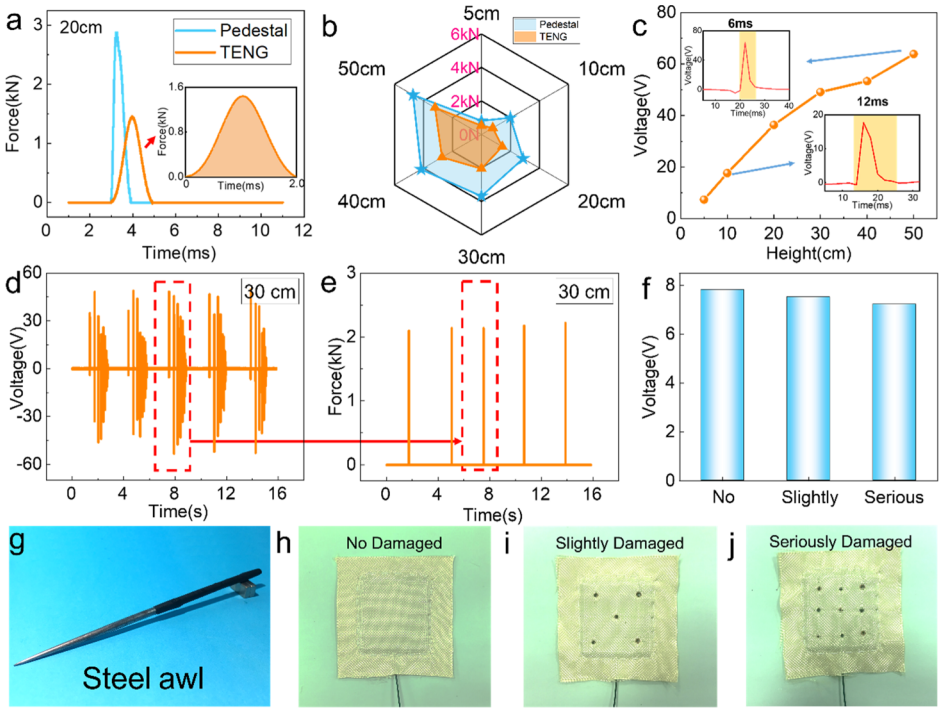

Figure 3. Typical force−time curves of SS-TENG and the force sensor with impactor falling from (a) 20 cm, dropping height-dependent (b) impact force and (c) voltage signals, (d) voltage and (e) impact force cycling stability of SS-TENG loaded from 30 cm, (h−j) SS-TENG was penetrated by (g) the awl impactor and the self-healing property of the inside c-SSG endowed SS-TENG with (f) stable outputting voltage signals.

c-SSG exhibited ideal stability under cyclic excitation frequencies of 0.1 and 100 Hz (Figure S2b).

On the other hand, the conductivity of c-SSG was dramatically improved as the CNT mass fraction increased (Figure 1d). Pure SSG was insulated and the impedance was 11.5 GΩ. However, it decreased to 0.1 MΩ when 1% CNT was introduced. If the CNT mass fraction increased to 3%, the impedance value was as low as 766.5 Ω. The stable current−voltage curve indicated its resistance was 0.6 kΩ (Figure S2c). Besides, a circuit composed of a battery, a light-emitting diode (LED), and c-SSG was applied to explore the self-healing property of the composite. c-SSG enabled to act as a conductive wire to help to light up an LED (Figure 1e). After cutting off c-SSG, the LED went out (Figure 1f). However, the bulb was lit again by reconnecting the two separated polymers, indicating its ideal self-healing property (Figure 1g). Based on the above results, c-SSG with CNTs of 3% was appropriate for further study.

Energy-Harvesting Performance of SS-TENG in Oscillator Compression Mode. The harvesting energy mechanism of SS-TENG in one cycle process is presented in Figure 2a. Based on the coupling effect of triboelectrification and electrostatic induction, the initial contact-induced charge transferred on the interface of PDMS and SS-TENG owing to their different electron affinity. It generated negative triboelectric charges on SS-TENG and positive ones on PDMS [Figure 2a(I)]. After the positive PDMS left, a potential difference between SS-TENG and the ground resulted in the flow of free electrons [Figure 2a(II)]. The system turned to electrostatic equilibrium when PDMS left far away and free electrons ran out [Figure 2a(III)]. Once PDMS approached Kevlar again, the increased potential in c-SSG could drive the free electrons to flow back from the ground, which generated a negative current signal until the system reversed to the initial state [Figure 2a(IV)]. This contact-separation movement was common in daily life. Therefore, the as-designed SS-TENG could be used to harvest mechanical energy and convert them into environmentally friendly electrical energy.

The resistance-dependent triboelectric performance of c-SSG/Kevlar-based SS-TENG was further systematically explored. The SS-TENG mentioned above is presented in Figure 2b. SS-TENG was attached on a flat panel and followed by excitation using an oscillator. A force sensor was installed near the probe of the oscillator to record the loading force. The contact force was set at 60 N and the frequency was 10 Hz. When the external resistance increased from 1 kΩ to 1 GΩ, the voltage signal measured using the digital multimeter increased from 6 mV to 24 V, while the current decreased from 6 to 0.02 μA (Figure 2c). The maximum peak power density reached 5.3 mW/m^2 with a voltage of 13.1 V under 9 MΩ (Figure 2d). Therefore, the SS-TENG device could act as a new power source to light up LED arrays (Figure 2e). On the other hand, the constant contact-separation loading frequency also showed a positive influence on the output performance of SS-TENG. For instance, voltages increased from 1.7 to 16.7 V as the loading frequencies vary from 1 to 10 Hz (Figure S3a).

Furthermore, the cycling stability of SS-TENG was explored owing to its importance in practical applications. Clearly, the output voltages exhibited favorable stability during 600 loading-unloading excitations at 9 MΩ (Figure 2f). For example, the voltage signal was 13.7 V during the 30−70 loadings (Figure 2g) while it changed to 15.3 V during the 530−570 cycles, increasing by 11.7% (Figure 2h). The current signal increased from 1.53 to 1.71 μA (Figure S3b). This slight increment was mainly because of the accumulation of electrons during cyclic loading−unloading compressions.

Safeguarding and Energy-Collecting Properties under Low Velocity Impact. Owing to the introduction of

https://dx.doi.org/10.1021/acsami.0c18308
ACS Appl. Mater. Interfaces 2021, 13, 6575−6584

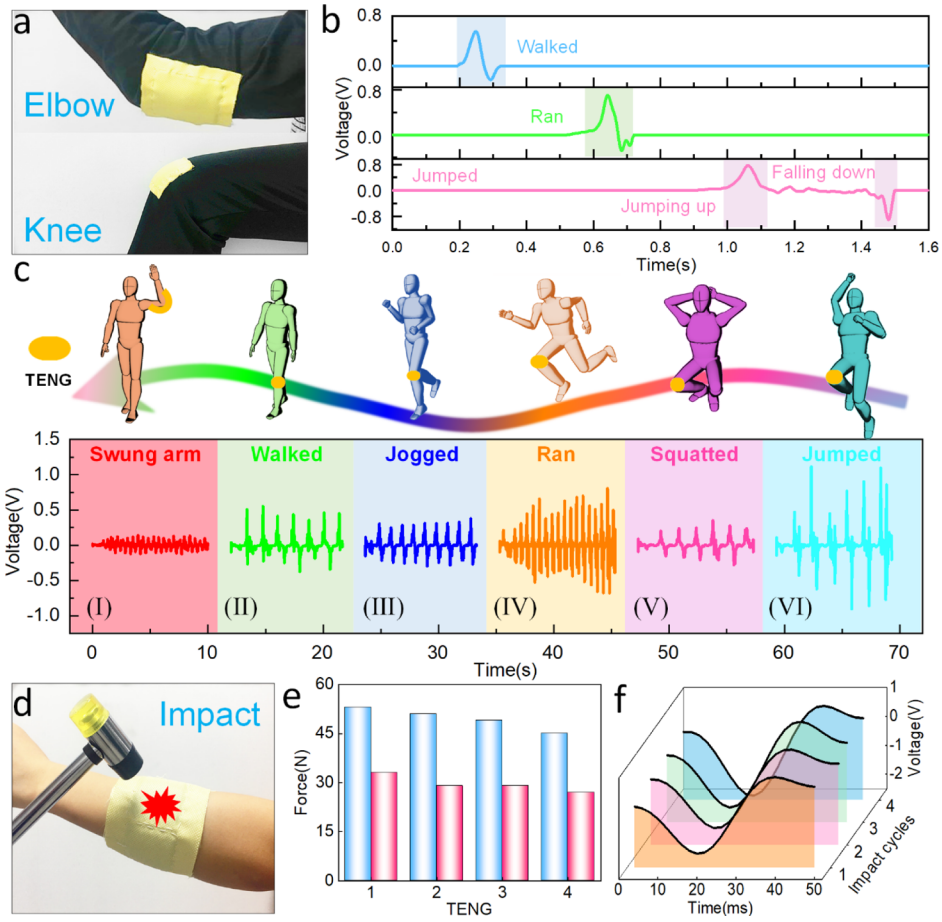

Figure 4. SS-TENG device could be worn on (a) elbow and knee. SS-TENG worked as self-powered flexible sensor to monitor human motions: (b) typical single voltage curves of walk, run, and jump; detecting various human motions including (c) swing arm, walking, jogging, running, squatting, and jumping; (d) SS-TENG on the wrist could provide protection for the wearer, the comparison of hammer impact forces loaded on the force sensor and SS-TENG, (e) force signal and (f) outputting voltage stability during cyclic impact on SS-TENG.

high energy-dissipating c-SSG, the safeguarding as well as energy-harvesting properties of c-SSG/Kevlar-based SS-TENG under low velocity impact were further explored using a drop hammer test system. SS-TENG was fixed on the metal force sensor, which could record the impact force after collision. Weight of the drop hammer was 0.5 kg. Impact force could be altered by changing the falling heights of impactor from 5 to 50 cm. When the falling height was 20 cm, the force directly impacting the force sensor was as high as 2880 N (Figure 3a). However, under the same conditions, the impact force loaded on SS-TENG was 1460 N. This indicated SS-TENG could decrease 49.3% of impact force, which provided protection for wearers. Besides, the buffering time also increased from 0.9 to 2 ms on SS-TENG. Similarly, under the falling from 50 cm, SS-TENG also exhibited great anti-impact properties (Figure S4a). Falling height-dependent impact force and the corresponding voltages are presented in Figure 3b,c, respectively. The impact force as well as outputting voltages increased with the increasing of dropping heights. Especially, when the falling height was 50 cm, impact force on SS-TENG was 3.2 kN (decreased by 32.2% compared with that on the force sensor) and the maximum voltage was 63.8 V, proving its energy-harvesting effect. These voltages also could be used to assess external impact excitations. On the other hand, the voltages (Figures S4b and 3d), current (Figure S5a,b), and impact forces (Figures S4c and 3e) of SS-TENG under the cyclic impact from 5 and 30 cm remained stable, which guaranteed its practical applications.

In consideration of the self-healing property of c-SSG, SS-TENG was penetrated and damaged to different degrees (Figure 3h–j) by the metal awl (Figure 3g). After self-healing for 5 min, the electrical properties under an impact force of 530 N were studied. Voltage of the pristine SS-TENG was 7.8 V. After damaging and healing, the values varied to 7.5 and 7.2 V, leading to 3.8 and 7.7% decrement. In conclusion, the reliable anti-impact, energy-collecting, and self-healing properties of Kevlar/c-SSG based-TENG under impact conditions ensured its application in new power sources, wearable sensors, and safeguards.

Human Behavior Monitoring Based on SS-TENG. Owing to the soft and high flexibility, c-SSG/Kevlar-based SS-TENG could be comfortably worn on the human body (Figure 4a) and showed promising application as a self-powered sensor to monitor various human movements. For example, typical voltage–time curves outputted by the SS-TENG on knee during human walking, running, and jumping were presented in Figure 4b. Surface contact between the knee and SS-TENG would produce an electrical signal and the maximum values during walking and running were 0.5 and 0.7 V, respectively. A positive voltage signal was produced when the person jumped and after falling down, a negative voltage peak was observed. Interestingly, a short period between the

https://dx.doi.org/10.1021/acsami.0c18308
ACS Appl. Mater. Interfaces 2021, 13, 6575–6584

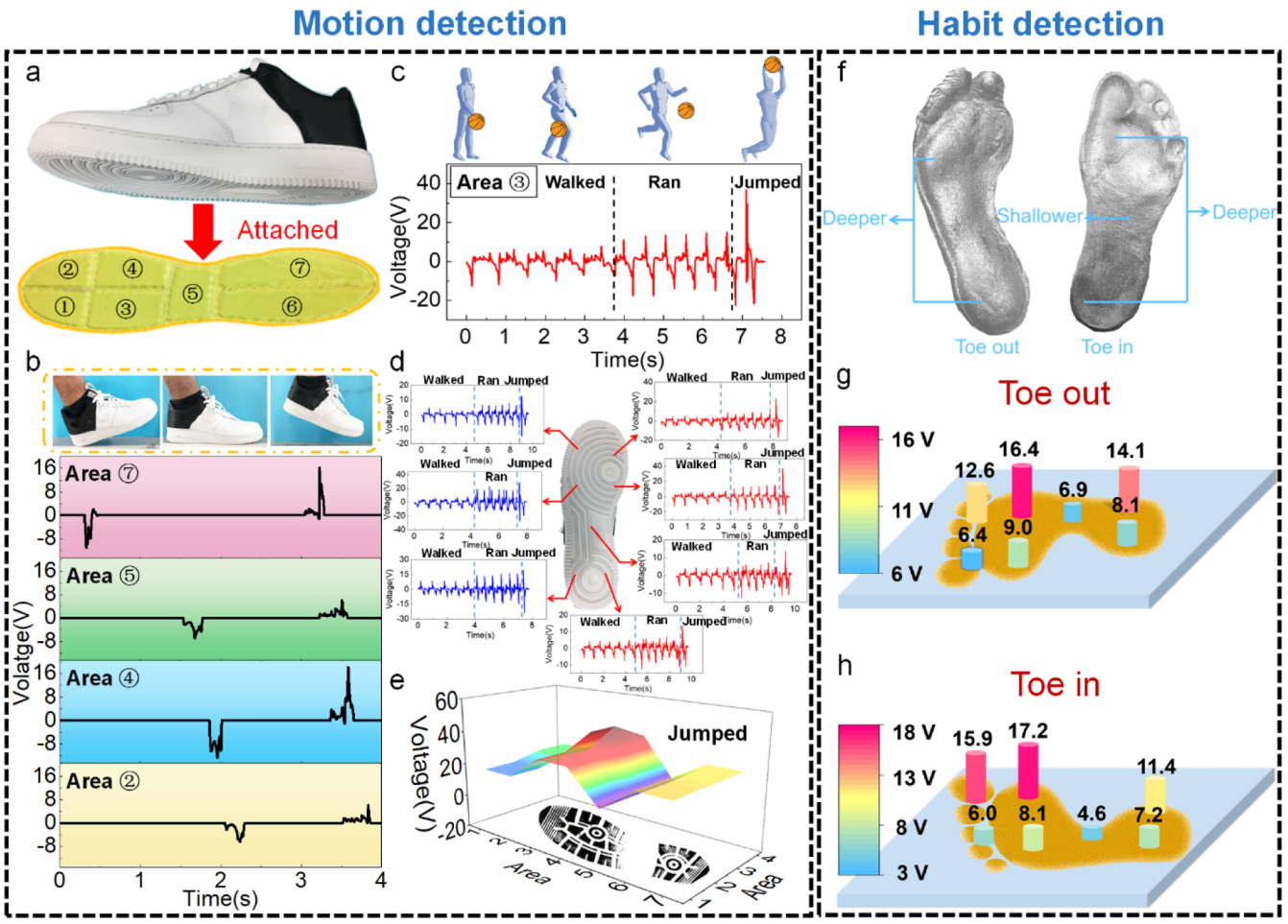

Figure 5. (a) SS-TENG-based sole array on the shoe; (b) electrical signals outputted by different units of the array during one process of human walk, (c) typical voltage−time curves generated by the "area 3" of the array to monitor various foot movements, (d) all the units of the array could assess the walking, running, and jumping processes, (e) voltage comparison of all units under jumping; (f) footprints in the imprint of different walking habits; and voltages of different areas under the shoes of (g) toe out and (h) toe in.

two voltage peaks could be used to assess the jumping speed and the time during jumping off and falling down.

Moreover, SS-TENG showed reliability in sensing various joint movements in Figure 4c. Especially, the average voltage values of jogging, squatting, and swinging arms were 315.9, 258.8, and 105.6 mV, respectively. SS-TENG also exhibited high sensitivity to different external excitations. It could record the low frequencies of walking [Figure 4c(II)], squatting [Figure 4c(V)], and jumping [Figure 4c(VI)]. Simultaneously, SS-TENG was able to sense higher-frequency motions such as jogging [Figure 4c(III)], running [Figure 4c(IV)], and swing arm [Figure 4c(I)].

More importantly, the wearable SS-TENG could be applied as a wrist protector and a force sensor under impact conditions (Figure 4d). A hammer was used to load the strike and the force sensor was fixed between human arm and SS-TENG enabled to record the impact force. During cyclic impact on the force sensor, the maximum force was about 53 N (Figure 4e). However, it reduced to 33 N owing to the energy-absorption effect of SS-TENG, suggesting the wearable device could protect human beings. Meanwhile, the self-powered voltages also showed high stability during the impact excitation, which remained at about −4 V (Figure 4f). To this end, the reported functional SS-TENG with self-powered sensing as well as safeguarding properties showed promising applications in sensors and human−machine interaction and personal safety areas.

TENG-Based Wearable Sole for Exercise Monitoring. Human feet were vital organs in daily life and many movements should rely on feet. Injury in feet may seriously influence our life and work. Thus, it was preferable to develop a novel SS-TENG array to monitor as well as protect feet during exercise. Because of the high sensitivity and a fast response to external impact, the as-designed SS-TENG showed potential application in exercise monitoring. Therefore, a SS-TENG-based sole array was developed by sewing different shapes of c-SSG into Kevlar. The array with various units was then attached to the shoe to detect human movements (Figure 5a). First, the sensing performance of the SS-TENG array during one process of human walk was studied. Once the heel touched the ground, unit 7 of the array started to output a voltage of −11.1 V at 0.3 s (Figure 5b). Then, units 5, 4, and 2 gradually generated −7.0, −12.7, and −6.3 V as feet stepped on the ground. Finally, the appearance of a positive signal on each unit indicated that foot left the ground. This result proved the as-designed SS-TENG array enabled consecutively and precisely detecting foot motions. Taking unit 3 as an example, it could sense the shooting basketball process of a player, which included walking, running, and jumping (Figure 5c). The voltage frequency of running was obviously much faster

https://dx.doi.org/10.1021/acsami.0c18308
ACS Appl. Mater. Interfaces 2021, 13, 6575−6584

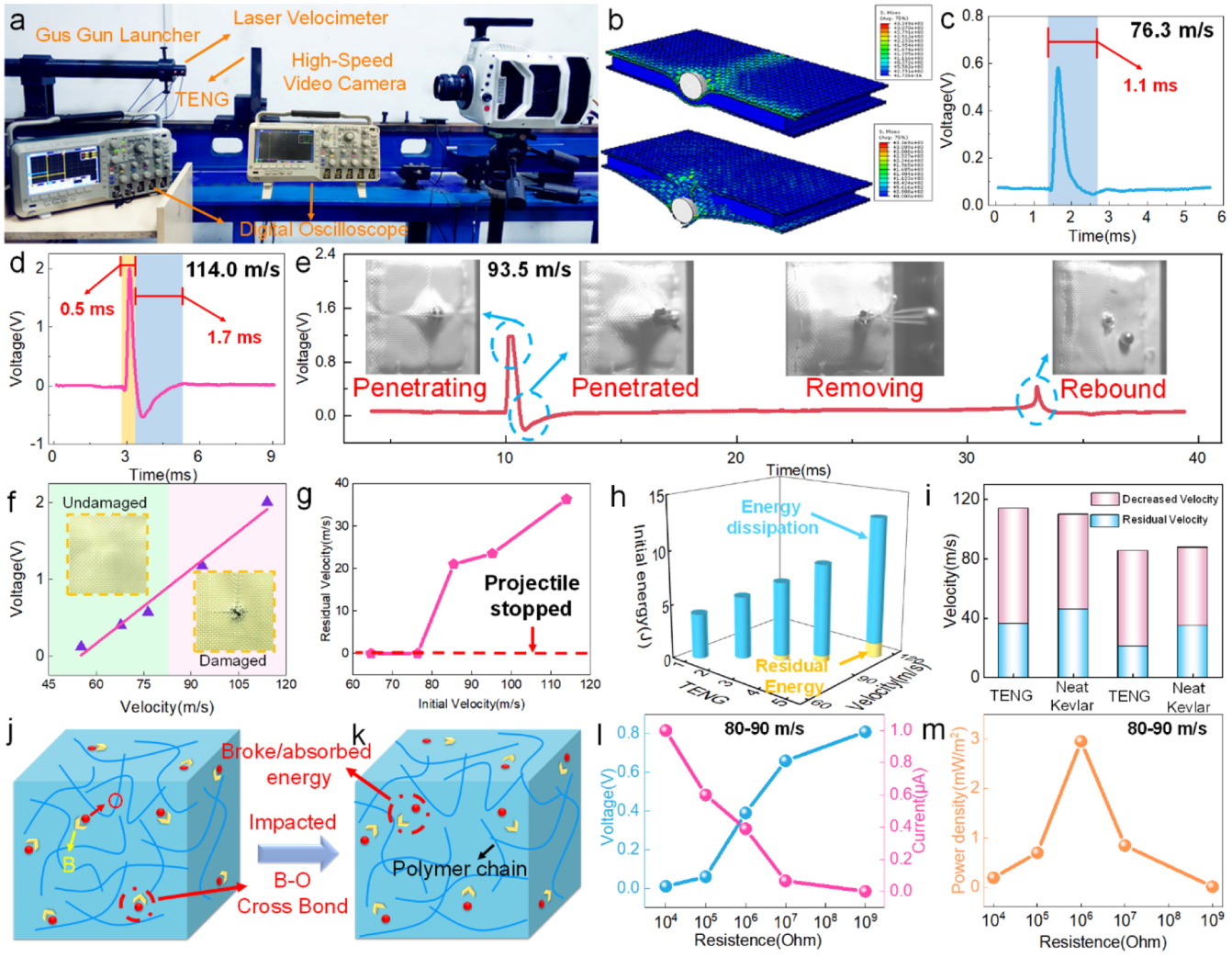

Figure 6. (a) Photos of the a high-velocity ballistic impact system; (b) simulation results of stress distribution on SS-TENG during shooting penetration; voltage signal of SS-TENG generated by the bullet impact with (c) 76.3 and (d) 114.0 m/s; (e) impact velocity-dependent voltage signals; (f) voltage signals of the bullet passed through SS-TENG and bounced back; the residual (g) velocity and (h) energy results of SS-TENG under the impact with various incident velocities; (i) corresponding bullet residual velocities of SS-TENG and neat Kevlar; (j,k) mechanism of the rate-dependent behavior of the c-SSG; energy-harvesting properties including (l) voltage, current, and (m) output power density under high speed impact conditions and the corresponding bullet residual velocities.

than those of walking and the maximum voltage during jumping was the largest. Similarly, other units of the array also could detect these series of movements (Figure 5d). However, the outputting voltages of all units under the same excitation were different, which was because of the varied pressures on sole. The voltage distribution map of the array under jumping is presented in Figure 5e. Clearly, unit 3 generated the maximum voltage of 39.7 V owing to its maximum sustaining pressures during jumping.

In addition, different people often had different walking styles in daily life, but some incorrect walking habits, such as toe out and toe in, were often not easy to perceive and potentially harmful. Thus, our designed sole array may help to monitor and correct these habits by recording and analyzing the voltage signals generated by the shoe sole sensor array. First, an adult stepped on the inkpad to mimic the walking style of toe in and toe out. From Figure 5f, the inside of the footprint of toe in waking habit was deeper, indicating these parts maintaining larger compression forces. As for walking of toe out, the outside of the footprint was under more pressure. Therefore, in consideration of the self-powered sensing performance of the sole array, the pressure distribution as well as the walking habits could be clearly monitored. From Figure 5g, units 2, 4, and 7 sustained more pressure and the corresponding voltages were 12.6, 16.4, and 14.1 V, which were higher than those of units 1, 3, and 6. On the other hand, if the outputting voltages of units 1, 3, and 6 were larger, this phenomenon indicated the people walked in toe in way (Figure 5h). In conclusion, these results proved the reported novel SS-TENG-based sole array with a fast response and a self-powered sensing effect could distinguish different foot motions, endowing its application in sports, health care and diagnosis.

Anti-impact Mechanical Performance and Energy Collection of c-SSG/Kevlar-Based SS-TENG under Ballistic Impact. Kevlar, as one of the most famous fiber materials, was applied in body armor owing to its high tensile modulus and excellent puncture resistance. Kevlar combined with a shear-stiffening composite was proven with better anti-impact performance.[32] Thus, it was essential to further explore

https://dx.doi.org/10.1021/acsami.0c18308
ACS Appl. Mater. Interfaces 2021, 13, 6575−6584

the safeguarding as well as energy-harvesting properties of c-SSG/Kevlar-based SS-TENG under high speed impact conditions. In this work, a ballistic impact testing system, which included a gas gun, a laser velocimeter, a digital oscilloscope, and a high-speed video camera, was applied to load the bullet impact excitation (Figure 6a). A spherical bullet with a diameter of 8.1 mm and a weight of 2 g was placed in the chamber of the gas gun. The initial velocity was controlled by the air pressure and depth of the bullet in the chamber. A laser velocimeter was attached to the muzzle of the air gun launcher and an oscilloscope was connected to measure the bullet's initial velocity. The SS-TENG was fixed on the clamp opposite to the muzzle and the conductive wire was connected to another oscilloscope used to record the electrical signal from the SS-TENG during the impact.

According to the finite element method simulations, it was the cross-shaped Kevlar fibers, which sustained the bullet-shooting force (Figure 6b). When subjecting to high speed impact, c-SSG showed a shear-stiffening effect, which also absorbed the impact energy and provided protection until the SS-TENG was totally penetrated. The SS-TENG could resist the ballistic shoot with a velocity of 76.3 m/s and there was only one voltage peak with 0.6 V owing to the one contact between the bullet and SS-TENG (Figure 6c). This duration was 1.1 ms. However, SS-TENG was totally penetrated when the velocity increased to 114 m/s. On this occasion, the voltage−time curve was remarkably different. A positive voltage of 2 V was generated as the bullet touched the SS-TENG and began to penetrate the fiber (Figure 6d). This duration lasted 0.5 ms. The followed negative voltage of −0.5 V was generated by the contact of the bullet and c-SSG. This process lasted 1.7 ms owing to the thicker c-SSG and the bullet speed also decreased. Figure 6e also presented a similar process with digital photos. As the bullet velocity decreased to 93.5 m/s, the maximum voltage also reduced to 1.2 V. However, when the bullet struck the protective panel and bounced back to re-contract the SS-TENG, a lower voltage of 0.4 V was observed. The shooting speed-dependent output voltage result is fitted in Figure 6f. Undoubtedly, the impact speed exhibited a positive influence on the output voltages and these electrical curves could also be used to assess external impact and judge the damage of the SS-TENG device. It was worth noting that SS-TENG could still respond to shocks after penetration and could continue to collect energy (Figure S6a).

In addition, the energy-harvesting properties under a high-speed shooting process were systematically investigated. Figure 6l presented the voltage and current of SS-TENG connected with various resistances in the impact speed range of 80−90 m/s. Clearly, the voltage increased with the increasing of resistance and current showed the opposite tendency. The instantaneous power density of SS-TENG first increased and then decreased (Figure 6m). The maximum power density was as high as 3 mW/m^2 and the current was 0.043 μA (Figure S6b) at a resistance of 1 MΩ. To this end, the wearable SS-TENG device exhibited enhanced anti-ballistic performance and excellent energy-gathering property under high speed shooting conditions, which endowed its application in smart body armors.

Besides, the residual velocity as well as absorbed energy of SS-TENG during the penetrating process were further explored. The SS-TENG device could totally maintain and impede the kinetic energy of bullets with 76.3 m/s and no penetration occurred. As the initial velocity changed to 95.2 m/s (kinetic energy of 9.1 J), the residual speed and energy were 23.5 m/s (Figure 6g) and 0.55 J. This also proved the SS-TENG device exhibited protection properties. In addition, the safeguarding property of SS-TENG and pure Kevlar was compared. As the initial shooting speed was about 114 m/s, the residual velocity penetrating SS-TENG and two layers of Kevlar were 36.3 and 46.0 m/s (Figure 6i), respectively. This enhancement in anti-impact property was mainly because of the addition of energy-dissipation of c-SSG. B atoms with the p orbit could attract the abundant electrons of the O atom to form a B−O cross bond (Figure 6j). During impact, large numbers of the B−O bonds interacted with each other to impede the movement of polymer chains (Figure 6k).[38,39] Therefore, c-SSG enabled absorbing and dissipating much kinetic energy during the penetration process.

CONCLUSIONS

This work reported a multifunctional SS-TENG with protective and impact kinetic energy-harvesting properties by combining Kevlar fiber with conductive SSG. As a power generation device, this SS-TENG could generate 5.3 mW/m^2 with a voltage of 13.1 V under oscillator compression. Based on the self-powered sensing performance, the wearable SS-TENG could monitor various human motions. Interestingly, the SS-TENG-based sole array even distinguished toe in/out motions. More importantly, the novel SS-TENG enabled providing protection for human beings, which reduced the impact forces from 2880 to 1460 N. Acting as a self-powered sensor, it stably outputted different voltages during dynamic impacts. Besides, the functional SS-TENG could collect bullet-shooting mechanical energy by generating a power density of 3 mW/m^2 with a resistance of 1 MΩ at a speed of 80−90 m/s. It also effectively resisted a shooting speed of 76.3 m/s owing to the enhancement of c-SSG. To this end, this SS-TENG with enhanced mechanical properties guaranteed its applications in new power sources, wearable sensors, and body armors.

ASSOCIATED CONTENT

Supporting Information

The Supporting Information is available free of charge at https://pubs.acs.org/doi/10.1021/acsami.0c18308.

TENG-based device could be used to detect human motions (Video S1) (MP4)

SEM micrographs of neat Kevlar, CNT, pure SSG and c-SSG; supplement to the rheological properties of c-SSG; frequency-dependent voltage and current cyclic stability of TENG; typical force−time curves from 50 cm and voltage and impact force cyclic stability of SS-TENG loaded from 5 cm; current signal cycling stability of TENG loaded from 5 and 30 cm; and SS-TENG-harvested mechanical energy after being penetrated and current signal generated by the bullet impact (PDF)

AUTHOR INFORMATION

Corresponding Authors

Sheng Wang − *CAS Key Laboratory of Mechanical Behavior and Design of Materials, Department of Modern Mechanics, CAS Center for Excellence in Complex System Mechanics, University of Science and Technology of China (USTC), Hefei 230027, P. R. China*; Email: wsh160@ustc.edu.cn

Xinglong Gong − *CAS Key Laboratory of Mechanical Behavior and Design of Materials, Department of Modern*

https://dx.doi.org/10.1021/acsami.0c18308
ACS Appl. Mater. Interfaces 2021, 13, 6575−6584

Mechanics, CAS Center for Excellence in Complex System Mechanics, University of Science and Technology of China (USTC), Hefei 230027, P. R. China; State Key Laboratory of Fire Science, University of Science and Technology of China, Hefei, Anhui 230026, PR China; orcid.org/0000-0001-6997-9526; Email: gongxl@ustc.edu.cn

Authors

Jianyu Zhou − *CAS Key Laboratory of Mechanical Behavior and Design of Materials, Department of Modern Mechanics, CAS Center for Excellence in Complex System Mechanics, University of Science and Technology of China (USTC), Hefei 230027, P. R. China*

Fang Yuan − *CAS Key Laboratory of Mechanical Behavior and Design of Materials, Department of Modern Mechanics, CAS Center for Excellence in Complex System Mechanics, University of Science and Technology of China (USTC), Hefei 230027, P. R. China*

Junshuo Zhang − *CAS Key Laboratory of Mechanical Behavior and Design of Materials, Department of Modern Mechanics, CAS Center for Excellence in Complex System Mechanics, University of Science and Technology of China (USTC), Hefei 230027, P. R. China*

Shuai Liu − *CAS Key Laboratory of Mechanical Behavior and Design of Materials, Department of Modern Mechanics, CAS Center for Excellence in Complex System Mechanics, University of Science and Technology of China (USTC), Hefei 230027, P. R. China*

Chunyu Zhao − *CAS Key Laboratory of Mechanical Behavior and Design of Materials, Department of Modern Mechanics, CAS Center for Excellence in Complex System Mechanics, University of Science and Technology of China (USTC), Hefei 230027, P. R. China*

Yu Wang − *CAS Key Laboratory of Mechanical Behavior and Design of Materials, Department of Modern Mechanics, CAS Center for Excellence in Complex System Mechanics, University of Science and Technology of China (USTC), Hefei 230027, P. R. China*

Complete contact information is available at: https://pubs.acs.org/10.1021/acsami.0c18308

Notes

The authors declare no competing financial interest.

■ ACKNOWLEDGMENTS

Financial support from the National Natural Science Foundation of China (grant nos. 11972032, 11802303, and 11772320), the Strategic Priority Research Program of the Chinese Academy of Sciences (grant no. XDB22040502), and China Postdoctoral Science Foundation (grant no. 2019T120544) is gratefully acknowledged.

■ ABBREVIATIONS

TENG, nanogenerator
SSG, shear-stiffening gel
c-SSG, conductive shear-stiffening gel
G'_{min}, initial storage modulus
G'_{max}, maximum storage modulus

■ REFERENCES

(1) Harper, G.; Sommerville, R.; Kendrick, E.; Driscoll, L.; Slater, P.; Stolkin, R.; Walton, A.; Christensen, P.; Heidrich, O.; Lambert, S.; Abbott, A.; Ryder, K.; Gaines, L.; Anderson, P. Recycling Lithium-ion Batteries from Electric Vehicles. *Nature* **2019**, *575*, 75−86.

(2) Shao, H.; Wu, Y.-C.; Lin, Z.; Taberna, P.-L.; Simon, P. Nanoporous Carbon for Electrochemical Capacitive Energy Storage. *Chem. Soc. Rev.* **2020**, *49*, 3005−3039.

(3) Hu, P.; Yan, M.; Zhu, T.; Wang, X.; Wei, X.; Li, J.; Zhou, L.; Li, Z.; Chen, L.; Mai, L. Zn/V_2O_5 Aqueous Hybrid-Ion Battery with High Voltage Platform and Long Cycle Life. *ACS Appl. Mater. Interfaces* **2017**, *9*, 42717−42722.

(4) Ott, J.; Völker, B.; Gan, Y.; McMeeking, R. M.; Kamlah, M. A Micromechanical Model for Effective Conductivity in Granular Electrode Structures. *Acta Mech. Sin.* **2013**, *29*, 682−698.

(5) Xiao, N.; McCulloch, W. D.; Wu, Y. Reversible Dendrite-Free Potassium Plating and Stripping Electrochemistry for Potassium Secondary Batteries. *J. Am. Chem. Soc.* **2017**, *139*, 9475−9478.

(6) Ning, S.; Zhang, S.; Sun, J.; Li, C.; Zheng, J.; Khalifa, Y. M.; Zhou, S.; Cao, J.; Wu, Y. Ambient Pressure X-ray Photoelectron Spectroscopy Investigation of Thermally Stable Halide Perovskite Solar Cells via Post-Treatment. *ACS Appl. Mater. Interfaces* **2020**, *12*, 43705−43713.

(7) Du, X.; Li, N.; Liu, Y.; Wang, J.; Yuan, Z.; Yin, Y.; Cao, R.; Zhao, S.; Wang, B.; Wang, Z. L.; Li, C. Ultra-robust Triboelectric Nanogenerator for Harvesting Rotary Mechanical Energy. *Nano Res.* **2018**, *11*, 2862−2871.

(8) Lee, J.-H.; Lee, K. Y.; Gupta, M. K.; Kim, T. Y.; Lee, D.-Y.; Oh, J.; Ryu, C.; Yoo, W. J.; Kang, C.-Y.; Yoon, S.-J.; Yoo, J.-B.; Kim, S.-W. Highly Stretchable Piezoelectric-Pyroelectric Hybrid Nanogenerator. *Adv. Mater.* **2014**, *26*, 765−769.

(9) Alluri, N. R.; Saravanakumar, B.; Kim, S.-J. Flexible, Hybrid Piezoelectric Film $(BaTi_{(1-x)}Zr_xO_3)$/PVDF Nanogenerator as a Self-Powered Fluid Velocity Sensor. *ACS Appl. Mater. Interfaces* **2015**, *7*, 9831−9840.

(10) Li, W.; Torres, D.; Diaz, R.; Wang, Z.; Wu, C.; Wang, C.; Wang, Z.; Sepulveda, N. Nanogenerator-based Dual-functional and Self-powered Thin Patch Loudspeaker or Microphone for Flexible Electronics. *Nat. Commun.* **2017**, *8*, 15310.

(11) Li, C.; Yin, Y.; Wang, B.; Zhou, T.; Wang, J.; Luo, J.; Tang, W.; Cao, R.; Yuan, Z.; Li, N.; Du, X.; Wang, C.; Zhao, S.; Liu, Y.; Wang, Z. L. Self-Powered Electrospinning System Driven by a Triboelectric Nanogenerator. *ACS Nano* **2017**, *11*, 10439−10445.

(12) Kwak, S. S.; Yoon, H.-J.; Kim, S.-W. Textile-Based Triboelectric Nanogenerators for Self-Powered Wearable Electronics. *Adv. Funct. Mater.* **2019**, *29*, 1804533−1804558.

(13) Zhou, T.; Zhang, C.; Han, C. B.; Fan, F. R.; Tang, W.; Wang, Z. L. Woven Structured Triboelectric Nanogenerator for Wearable Devices. *ACS Appl. Mater. Interfaces* **2014**, *6*, 14695−14701.

(14) Yan, C.; Deng, W.; Jin, L.; Yang, T.; Wang, Z.; Chu, X.; Su, H.; Chen, J.; Yang, W. Epidermis-Inspired Ultrathin 3D Cellular Sensor Array for Self-Powered Biomedical Monitoring. *ACS Appl. Mater. Interfaces* **2018**, *10*, 41070−41075.

(15) Chen, X.; Parida, K.; Wang, J.; Xiong, J.; Lin, M.-F.; Shao, J.; Lee, P. S. A Stretchable and Transparent Nanocomposite Nanogenerator for Self-Powered Physiological Monitoring. *ACS Appl. Mater. Interfaces* **2017**, *9*, 42200−42209.

(16) Cui, N.; Liu, J.; Gu, L.; Bai, S.; Chen, X.; Qin, Y. Wearable Triboelectric Generator for Powering the Portable Electronic Devices. *ACS Appl. Mater. Interfaces* **2015**, *7*, 18225−18230.

(17) Zhu, M.; Shi, Q.; He, T.; Yi, Z.; Ma, Y.; Yang, B.; Chen, T.; Lee, C. Self-Powered and Self-Functional Cotton Sock Using Piezoelectric and Triboelectric Hybrid Mechanism for Healthcare and Sports Monitoring. *ACS Nano* **2019**, *13*, 1940−1952.

(18) Zhao, Z.; Huang, Q.; Yan, C.; Liu, Y.; Zeng, X.; Wei, X.; Hu, Y.; Zheng, Z. Machine-washable and Breathable Pressure Sensors Based on Triboelectric Nanogenerators Enabled by Textile Technologies. *Nano Energy* **2020**, *70*, 104528−104535.

(19) Chiu, C.-M.; Ke, Y.-Y.; Chou, T.-M.; Lin, Y.-J.; Yang, P.-K.; Wu, C.-C.; Lin, Z.-H. Self-powered Active Antibacterial Clothing Through Hybrid Effects of Nanowire-enhanced Electric Field

Electroporation and Controllable Hydrogen Peroxide Generation. *Nano Energy* **2018**, *53*, 1−10.
(20) Ma, L.; Wu, R.; Liu, S.; Patil, A.; Gong, H.; Yi, J.; Sheng, F.; Zhang, Y.; Wang, J.; Wang, J.; Guo, W.; Wang, Z. L. A Machine-Fabricated 3D Honeycomb-Structured Flame-Retardant Triboelectric Fabric for Fire Escape and Rescue. *Adv. Mater.* **2020**, *32*, 2003897.
(21) Yang, R.; Qin, Y.; Li, C.; Zhu, G.; Wang, Z. L. Converting Biomechanical Energy into Electricity by a Muscle-Movement-Driven Nanogenerator. *Nano Lett.* **2009**, *9*, 1201−1205.
(22) Lee, J. H.; Kim, S.; Kim, T. Y.; Khan, U.; Kim, S.-W. Water Droplet-driven Triboelectric Nanogenerator with Superhydrophobic Surfaces. *Nano Energy* **2019**, *58*, 579−584.
(23) Bian, Y.; Jiang, T.; Xiao, T.; Gong, W.; Cao, X.; Wang, Z.; Wang, Z. L. Triboelectric Nanogenerator Tree for Harvesting Wind Energy and Illuminating in Subway Tunnel. *Adv. Mater. Technol.* **2018**, *3*, 1700317−1700341.
(24) Helgeson, M. E.; Porcar, L.; Lopez-Barron, C.; Wagner, N. J. Direct Observation of Flow-Concentration Coupling in a Shear-Banding Fluid. *Phys. Rev. Lett.* **2010**, *105*, 084501.
(25) Lee, Y.-F.; Luo, Y.; Brown, S. C.; Wagner, N. J. Experimental Test of a Frictional Contact Model for Shear Thickening in Concentrated Colloidal Suspensions. *J. Rheol.* **2020**, *64*, 267−282.
(26) Gürgen, S.; Kuşhan, M. C.; Li, W. Shear Thickening Fluids in Protective Applications: A review. *Prog. Polym. Sci.* **2017**, *75*, 48−72.
(27) Wang, S.; Jiang, W.; Jiang, W.; Ye, F.; Mao, Y.; Xuan, S.; Gong, X. Multifunctional Polymer Composite with Excellent Shear Stiffening Performance and Magnetorheological Effect. *J. Mater. Chem. C* **2014**, *2*, 7133−7140.
(28) Li, D.; Wang, R.; Liu, X.; Fang, S.; Sun, Y. Shear-Thickening Fluid Using Oxygen-Plasma-Modified Multi-Walled Carbon Nanotubes to Improve the Quasi-Static Stab Resistance of Kevlar Fabrics. *Polymers* **2018**, *10*, 1356−1368.
(29) Gokuldass, R.; Ramesh, R. Mechanical and Low Velocity Impact Behaviour of Intra-ply Glass/kevlar Fibre Reinforced Nano-silica and Micro-rubber Modified Epoxy Resin Hybrid Composite. *Mater. Res. Express* **2019**, *6*, 055302−055311.
(30) Kalman, D. P.; Merrill, R. L.; Wagner, N. J.; Wetzel, E. D. Effect of Particle Hardness on the Penetration Behavior of Fabrics Intercalated with Dry Particles and Concentrated Particle-Fluid Suspensions. *ACS Appl. Mater. Interfaces* **2009**, *1*, 2602−2612.
(31) Tan, Z.; Li, W.; Huang, W. The Effect of Graphene on the Yarn Pull-out Force and Ballistic Performance of Kevlar Fabrics Impregnated with Shear Thickening Fluids. *Smart Mater. Struct.* **2018**, *27*, 075048.
(32) Wang, S.; Xuan, S.; Liu, M.; Bai, L.; Zhang, S.; Sang, M.; Jiang, W.; Gong, X. Smart Wearable Kevlar-based Safeguarding Electronic Textile with Excellent Sensing Performance. *Soft Matter* **2017**, *13*, 2483−2491.
(33) Zhang, S. L.; Lai, Y.-C.; He, X.; Liu, R.; Zi, Y.; Wang, Z. L. Auxetic Foam-Based Contact-Mode T riboelectric Nanogenerator with Highly Sensitive Self-Powered Strain Sensing Capabilities to Monitor Human Body Movement. *Adv. Funct. Mater.* **2017**, *27*, 1606695.
(34) Chen, H.; Bai, L.; Li, T.; Zhao, C.; Zhang, J.; Zhang, N.; Song, G.; Gan, Q.; Xu, Y. Wearable and Robust Triboelectric Nanogenerator Based on Crumpled Gold Films. *Nano Energy* **2018**, *46*, 73−80.
(35) Wu, H.; Chen, Z.; Xu, G.; Xu, J.; Wang, Z.; Zi, Y. Fully Biodegradable Water Droplet Energy Harvester Based on Leaves of Living Plants. *ACS Appl. Mater. Interfaces* **2020**, *12*, 56060−56067.
(36) Deng, J.; Kuang, X.; Liu, R.; Ding, W.; Wang, A. C.; Lai, Y.-C.; Dong, K.; Wen, Z.; Wang, Y.; Wang, L.; Qi, H. J.; Zhang, T.; Wang, Z. L. Vitrimer Elastomer-Based Jigsaw Puzzle-Like Healable Triboelectric Nanogenerator for Self-Powered Wearable Electronics. *Adv. Mater.* **2018**, *30*, 1705918.
(37) Sun, J.; Pu, X.; Liu, M.; Yu, A.; Du, C.; Zhai, J.; Hu, W.; Wang, Z. L. Self-Healable, Stretchable, Transparent Triboelectric Nanogenerators as Soft Power Sources. *ACS Nano* **2018**, *12*, 6147−6155.
(38) Wang, S.; Gong, L.; Shang, Z.; Ding, L.; Yin, G.; Jiang, W.; Gong, X.; Xuan, S. Novel Safeguarding Tactile e-Skins for Monitoring Human Motion Based on SST/PDMS-AgNW-PET Hybrid Structures. *Adv. Funct. Mater.* **2018**, *28*, 1707538−1707546.
(39) Wang, S.; Xuan, S.; Jiang, W.; Jiang, W.; Yan, L.; Mao, Y.; Liu, M.; Gong, X. Rate-dependent and Self-healing Conductive Shear Stiffening Nanocomposite: A Novel Safe-guarding Material with Force Sensitivity. *J. Mater. Chem. A* **2015**, *3*, 19790−19799.

https://dx.doi.org/10.1021/acsami.0c18308
ACS Appl. Mater. Interfaces 2021, 13, 6575−6584